Ostwald Ripening of Clusters during Protein Crystallization

Aaron M. Streets[1] and Stephen R. Quake[1,2,*]

[1]Department of Applied Physics, Stanford University, Stanford, California 94305, USA
[2]Department of Bioengineering and Howard Hughes Medical Institute, Stanford University, Stanford, California 94305, USA

(Received 4 November 2009; published 26 April 2010)

Contrary to classical nucleation theory, protein crystals can nucleate via a two-step process in which the molecular arrangement of the ordered solid phase is preceded by nucleation of a dense amorphous phase. We study the growth of these precrystalline clusters in lysozyme using a combination of dynamic light scattering, optical microscopy, and microfluidics. Clusters display Ostwald ripening growth kinetics but deviate from this trend after nucleation of the crystal phase. This behavior arises from the metastable relationship between clusters and the ordered solid and is explained numerically using a population balance model.

DOI: 10.1103/PhysRevLett.104.178102 PACS numbers: 87.15.Zg, 64.75.Gh, 81.10.−h

The formation of an ordered solid phase from aqueous solution is of particular importance in structural biology, where protein crystals of high purity are necessary for x-ray diffraction studies. However, the complex interaction potentials of biological macromolecules have challenged the formulation of a predictive theory of protein crystallization [1]. Thus great effort has been spent on developing a more complete understanding of this phase transition [2–11].

Theoretical and computational studies on model systems postulated a two-step nucleation mechanism in which molecular arrangement of the ordered solid phase is preceded by nucleation of a dense amorphous phase [2,3]. Experimental studies have observed this phase in the form of dense liquidlike clusters in both colloidal systems [4,5] and globular protein solutions [6]. There has since been increasing interest in the nature of this dense cluster phase and its effect on crystal nucleation rates [7–9]. However, little is known about the growth kinetics of these clusters themselves. Additionally, a better understanding of the relationship between this intermediate phase and crystal growth is in principle valuable for controlling crystal growth to achieve increased purity [10,11]. In this Letter we investigate the role of Ostwald ripening in the evolution of protein clusters in order to gain insight into how they interact with protein crystals.

Typically, Ostwald ripening occurs in the late stages of a first order phase transition [12]. After nucleation and growth of the new phase, minimization of total interfacial energy drives competitive growth between precipitate clusters of various sizes: smaller clusters account for a higher surface energy per unit volume and are ''devoured'' by the larger clusters. Ostwald ripening has been measured in many inorganic systems [13], and has been qualitatively observed in some macromolecule crystal systems [14,15]. However, its role in protein crystallization is less well understood.

The precrystalline dense phase plays an important role in the crystallization of hen egg-white lysozyme (HEWL), a model protein for crystallization studies [11]. We built a microfluidic dynamic light scattering (DLS) apparatus in order to characterize growth kinetics of these submicron precipitate populations involved in the crystallization of HEWL. DLS was used to measure hydrodynamic radii of populations of small precrystalline clusters while an integrated microscope simultaneously recorded images of larger nondiffusing crystals, yielding a dynamic range that extends from a few nanometers to hundreds of microns. This apparatus allows us to measure ripening of the clusters and observe the subsequent interaction between the cluster and crystal phase.

To model the evolution of the cluster size distribution (CSD) one can consider a distribution of spherical clusters where the competition between cluster surface curvature and volume defines a unique aqueous phase equilibrium concentration for each cluster of radius R. This cluster solubility is given by the Gibbs-Thomson relation, such that the solute concentration at the surface of the cluster is

$$C_{\mathrm{eq}}(R) = C_\infty \exp(\alpha/R) \tag{1}$$

and $\alpha = 2\gamma v_m/kT$ is the capillary length, γ is surface tension, and v_m is the solute molar volume. For any given monomer concentration $c(t)$, there will be a population of clusters which are out of equilibrium and will thus either dissolve or grow. The rate of cluster growth from transport of monomers to or from the cluster surface can be determined by Fickian diffusion [16]:

$$\frac{dR}{dt} = \frac{Dv_m}{R}[c(t) - C_{\mathrm{eq}}(R)], \tag{2}$$

where D is the monomer diffusion coefficient. By combining a linear approximation of Eq. (1), given $\alpha \ll R$, and Eq. (2) one can identify a critical radius $R_C = C_\infty \alpha/\Delta(t)$ where $\Delta(t)$ is the supersaturation $c(t) - C_\infty$. This result summarizes the ripening phenomenon: clusters of radius $R < R_C$ have $dR/dt < 0$ and will dissolve, releasing solute monomers to supply the growth of clusters with $R > R_C$.

The first quantitative treatment of Ostwald ripening was independently formulated by Lifshitz and Slyozov [17] and Wagner [18] (LSW) from first principles. They evaluated the time evolution of the CSD by noting that the number of clusters per unit volume with radius between R and $R + dR$, $n(R, t)$, is continuous in R space

$$\frac{\partial}{\partial t} n(R, t) + \frac{\partial}{\partial R}\left[n(R, t) \frac{dR}{dt} \right] = 0, \tag{3}$$

where dR/dt is given in Eq. (2), and by enforcing mass conservation

$$c(t) = c_0 - \frac{4\pi}{3 v_m} \int R^3 n(R, t) dR. \tag{4}$$

The concentration at any time $c(t)$ is the difference of the original concentration c_o and the total concentration in solid phase, represented by the integral term. Using Eqs. (2)–(4) LSW analytically calculated the moments of $n(R, t)$ in the asymptotic limit. They showed that the distribution mean size and number density depend on time as $t^{1/3}$ and t^{-1}, respectively. Many studies since LSW have reevaluated the ripening phenomena [16,19] and solved the system both numerically [20] and with computer simulations [19,21]. We compare both analytic predictions of ripening rates and simulated CSD evolution to light scattering and microscopy data.

We used microfluidic free-interface diffusion to induce HEWL crystallization as described in Ref. [22]. The microfluidic device is incorporated into a homemade light scattering system in which a 5 mW, 633 nm laser (Melles Griot) is focused to a 30 μm diameter spot in the middle of the protein chamber. Scattered photons are collected at a 60° angle and coupled to a single-mode fiber (Thorlabs) which delivers the signal to a photon counting module (Perkin Elmer). In addition to allowing a more convenient placement of the photon counting module (PCM), the single-mode fiber acts as a mode filter and improves the signal to noise of the dynamic light scattering measurement [23]. Photon arrival events are digitized by the PCM and then counted by a National Instruments PCI card and a PC. Autocorrelation functions were computed with custom written Labview software. The mean of CSDs were calculated with cumulant analysis [24] of the autocorrelation function and the distributions were solved directly using CONTIN [25].

HEWL stock was purchased from Hampton Research and dissolved to 100 mg/ml in a 0.05 mM sodium acetate buffer at 6.5 pH and sodium chloride was used as a crystallizing agent. Immediately after free-interface diffusion was initiated, CSDs were extracted from light scattering data and optical micrographs recorded every 2 min for 10 h. This allows continuous monitoring of the size distribution of submicron clusters as well as visible crystals. Matlab based image analysis software calculated the individual and total crystal area to measure the total protein mass in crystal phase as well as crystal growth rates similar to techniques employed in Ref. [26].

Figure 1(a) shows time courses of both the mean cluster hydrodynamic radius obtained by light scattering and the simultaneous growth of macroscopic crystal observed with optical microscopy. The conditions chosen ([lysozyme] = 60 mg/ml, [NaCl] = 0.6 M at equilibrium) yield growth of a few large tetragonal crystals in hours, but within minutes the cluster population enters the growth stage. Here, the mean cluster size evolution does not follow the asymptotic $t^{1/3}$ growth predicted by LSW or any other monotonic growth law proposed in previous crystal growth studies. Instead we observe a peak in the mean cluster size around 140 min followed by a slow decrease. The decrease in the mean size of clusters probed by DLS coincides with the emergence of visible HEWL crystals [Fig. 1(b)].

To elucidate the relationship between crystals and clusters the NaCl concentration was lowered to 0.5 M, such that typically either one or no crystals nucleate in a 10 h observation period. Figure 2 compares the mean cluster size evolution for two such reactions. In one experiment (open triangles) a single crystal appeared at 74 min and grows to almost full size in 10 h [Fig. 2 (inset)]. In the second experiment no crystal appeared in the 10 h time course (open circles). The respective effects of large crystal nucleation on the CSD differ significantly. When the emergence of a large crystal is observed the CSD evolution mimics the data in Fig. 1; a decrease in mean radius of the bulk CSD coincides with the growth of the large crystal. When the crystal phase fails to nucleate (and thus there is no significant depletion of the aqueous phase) the CSD mean does not peak and instead can be fit with power law growth (thin black line in Fig. 2) giving an exponent equal to 0.325, in close agreement with the 1/3 exponent predicted by LSW theory.

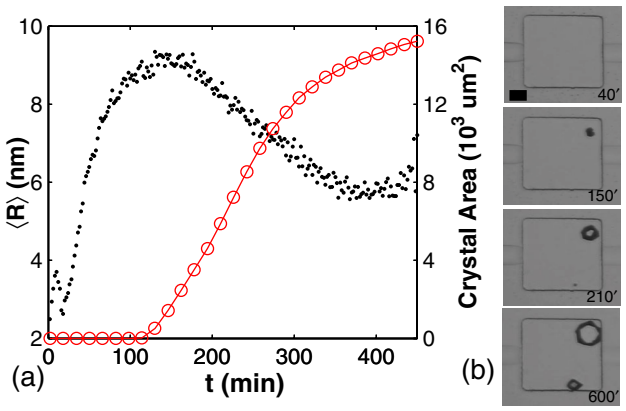

FIG. 1 (color online). (a) Mean cluster hydrodynamic radius from cumulant fit (●) with macrocrystal area (○). (b) Time lapse images of tetragonal HEWL crystal growth in microfluidic FID chambers at 40, 150, 210, and 600 min. The scale bar represents 100 um [27].

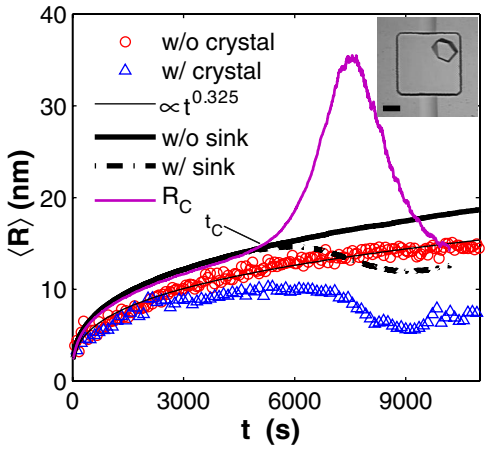

FIG. 2 (color online). Comparison of two experimental data sets with simulation. Crystal conditions are [HEWL] = 60 mg/ml, [NaCl] = 0.5 M for both data sets. In one experiment a single crystal formed after 74 min (△). In the other, no crystals formed in a 10 h period (○). Power law (thin black line) fit to the open circles gives $r = 2.82t^{0.325}$. Simulated mean radius evolution with a depletion term (dot-dashed line) and without (thick solid line). Simulated critical radius R_C (thin purple line). Final single crystal from open triangle set (inset) scale bar = 100 um.

In order to understand the deviation from the LSW model, two important assumptions about all present phases must be noted: (1) molecular deposition onto the surface of a new phase is a diffusion limited process and (2) the surface free energy can be approximated by the surface tension of a spherical cluster of protein monomers. Neither of these assumptions is valid for a tetragonal HEWL crystal. On the contrary, in faceted crystal growth, monomer deposition is often an interface kinetic limited process, and surface free energy is related to the chemical potential of the crystalline structure. The growth rate (and dissolution rate) of a crystal face is instead determined by the density of available incorporation sites and by the kinetic barrier to incorporation [10]. Amorphous clusters are thus metastable with respect to the crystal phase [6]. A critical fluctuation along the structure order parameter within the dense phase enables nucleation of the more stable crystal phase [3], after which, crystal growth dominates.

The crystals grow rapidly with respect to the protein clusters, and interact with the CSD by depleting the system of protein in solution. These large crystals can be thought of as a protein "sink" which decreases $c(t)$, in Eq. (2), thereby increasing the critical radius R_C. The peak in mean radius in Figs. 1 and 2 (open triangles) can be understood as the point at which R_C overcomes the mean cluster size, as described by Lifshitz and Slyozov.

We model this ripening phenomenon with a simple simulation to verify our qualitative explanation of the observation in Fig. 1. The simulation was modified from a population balance model game developed by De Smet *et al.* [21] in which at every step, monomers are added or subtracted to each cluster at a rate proportional to their respective solubility determined by Eq. (1). The simulation steps are as follows. First a distribution of N clusters is defined, with radii R_i where $i = 1, 2, \ldots, N$. Each cluster is filled with n_i molecules given molar volume v_m and for every simulation step j, n_i is adjusted at a rate $dn_i/dt = K_{ij}(R_i, R_C)$. This rate comes from substituting C_{eq} from Eq. (1) into Eq. (2) which yields

$$\frac{dn_i}{dt} = 4\pi D C_\infty \alpha N_A \left(\frac{R_i}{R_C} - 1\right). \tag{5}$$

For the case where no macrocrystal is present, mass conservation is implemented by imposing $\sum_i [K_{ij}] = 0$ which defines the critical radius $R_C = \sum_i [R_i/N]$.

The simulation was carried out on an initial log-normal cluster size distribution with mean $\langle r \rangle = 2.5$ nm, width $\sigma = 0.05$, and $N_o = 50\,000$ initial clusters. The mean radius fit with very high confidence ($R^2 = 0.99$) to power law growth with exponent equal to 0.33, and the cluster number density exhibits t^{-1} time dependence as predicted by LSW theory (not shown).

We modeled the effect of an emerging crystal by incorporating a depletion term into the simulation such that protein monomers are extracted from the system at a rate determined by the observed crystal growth, $P_j = -dn/dt$. The microscopy data in Fig. 1 were used to calculate this protein mass consumption rate of the crystal phase. Protein mass in crystal phase was approximated as a sigmoid in time, for the simulation, and the depletion term P_j takes the form of the sigmoid time derivative with units of molecules sec^{-1}. The mass balance equation then becomes $\sum_i [K_{ij}] = P_j$ and $R_C = \sum_i [R_i/(N - P_j)]$.

Figure 2 shows the results of the simulation, with and without a protein sink. The simulated mean cluster radii provide an accurate qualitative description of the experimental data, and with no adjustable parameters the simulated curves agree with the observed cluster evolution to within a factor of 2. The incorporation of the depletion term had a dramatic effect on the simulated CSD. The increased critical radius R_C (Fig. 2) which comes from a rapidly growing crystal, causes a maximum in mean cluster size, as observed in the experiment (open triangles). As the macrocrystal growth slows, the critical radius and CSD mean merge and approach a steady state. Thus, considering the crystal as a protein sink within the LSW model is sufficient to describe the time evolution of the amorphous cluster distribution.

Figure 3 shows the evolution of the CSD calculated with CONTIN from the same light scattering data used in Fig. 1 and compares the experimental distributions with simulated CSDs. We define time t_C as the point at which the critical radius R_C overcomes the mean radius as shown in Fig. 2. The simulated CSDs with and without a sink term are virtually identical when $t < t_C$, [Fig. 3(a)], and con-

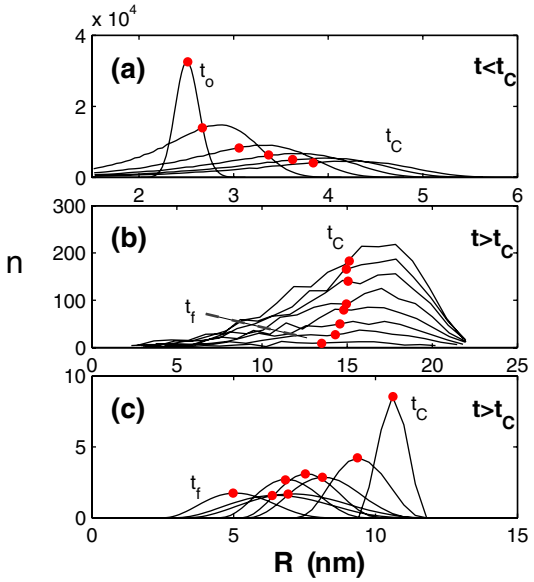

FIG. 3 (color online). Simulated and measured cluster size distributions. (a) Simulated distribution evolution for $t < t_C$ where t_C is the time at which R_C overtakes $\langle R \rangle$ (see Fig. 2). (b) Simulated distribution evolution with sink term for $t > t_C$. (c) CONTIN analysis of CSD for $t > t_C$ in the experiment from Fig. 1. CONTIN distributions are normalized to scattered intensity. Distribution mean is indicated with (●).

verge onto a self-similar distribution defined by LSW. With a sink term [Fig. 3(b)] the simulated distributions continue to broaden and flatten for $t > t_C$ [Fig. 3(b)], a common characteristic of Ostwald ripening [20], while the mean decreases as reflected in Fig. 2. CONTIN analysis of the light scattering data in Fig. 1 reveals a much more drastic evolution in the $t > t_C$ regime [Fig. 3(c)]. The data reflect the distribution broadening and decrease in mean radius predicted by the simulation; however, the observed CSDs have not yet converged to a self-similar distribution. This delayed convergence may be indication of transient ripening [19].

In this Letter we use Ostwald ripening formalism to explain the growth of precrystal protein clusters. Our measurements of CSD growth rates in lysozyme crystallization agree with simulations and analytic predictions of LSW theory. While the simplified model does not inherently account for competitive growth between clusters and the crystal phase, interpreting the crystal as a protein sink suffices to explain observed CSD evolution. The data here show that a crystal nucleation event is essentially ''recorded'' in the equilibrium cluster size distribution. The metastability of the cluster phase is revealed with nucleation of the crystal phase by a sudden decrease in mean cluster size. This may present an alternative way of measuring nucleation rates, a phenomenon which has yet to be directly observed in protein crystallization.

The authors would like to thank John Ross and Daniel Fisher for insightful discussions and the NIH Director's Pioneer grant for funding.

*To whom correspondence should be addressed.
quake@stanford.edu

[1] A. McPherson, *Crystallization of Biological Macromolecules* (Cold Spring Harbor Laboratory Press, Cold Spring Harbor, New York, 1999).
[2] P. R. t. Wolde and D. Frenkel, Science **277**, 1975 (1997).
[3] V. Talanquer and D. W. Oxtoby, J. Chem. Phys. **109**, 223 (1998).
[4] E. K. Hobbie, Phys. Rev. Lett. **81**, 3996 (1998).
[5] A. Stradner *et al.*, Nature (London) **432**, 492 (2004).
[6] P. G. Vekilov *et al.*, in *Aspects of Physical Biology* (Springer-Verlag, Berlin, Heidelberg, 2008), p. 65.
[7] J. F. Lutsko and G. Nicolis, Phys. Rev. Lett. **96**, 046102 (2006).
[8] J. R. Savage and A. D. Dinsmore, Phys. Rev. Lett. **102**, 198302 (2009).
[9] F. Sciortino *et al.*, Phys. Rev. Lett. **93**, 055701 (2004).
[10] P. G. Vekilov, Cryst. Growth Des. **7**, 2796 (2007).
[11] M. Muschol and F. Rosenberger, J. Chem. Phys. **107**, 1953 (1997).
[12] W. Ostwald, *Lehrbuch der Allgemeinen Chemie* (W. Engelmann, Leipzig, 1886), Vol. 2.
[13] P. W. Voorhees, Annu. Rev. Mater. Sci. **22**, 197 (1992).
[14] A. J. Malkin and A. McPherson, J. Cryst. Growth **126**, 555 (1993).
[15] J. D. Ng *et al.*, J. Cryst. Growth **168**, 50 (1996).
[16] J. A. Marqusee and J. Ross, J. Chem. Phys. **79**, 373 (1983).
[17] I. M. Lifshitz and V. V. Slyozov, J. Phys. Chem. Solids **19**, 35 (1961).
[18] C. Wagner, Z. Elektrochem. **65**, 581 (1961).
[19] J. Alkemper *et al.*, Phys. Rev. Lett. **82**, 2725 (1999).
[20] G. Madras and B. J. McCoy, Chem. Eng. Sci. **58**, 2903 (2003).
[21] Y. De Smet, L. Deriemaeker, and R. Finsy, Langmuir **13**, 6884 (1997).
[22] C. L. Hansen *et al.*, Proc. Natl. Acad. Sci. U.S.A. **99**, 16531 (2002).
[23] J. Ricka, Appl. Opt. **32**, 2860 (1993).
[24] D. E. Koppel, J. Chem. Phys. **57**, 4814 (1972).
[25] S. W. Provencher, Comput. Phys. Commun. **27**, 229 (1982).
[26] N. C. Bartelt, W. Theis, and R. M. Tromp, Phys. Rev. B **54**, 11741 (1996).
[27] See supplementary material at http://link.aps.org/supplemental/10.1103/PhysRevLett.104.178102 for an online video.